PASJ: Publ. Astron. Soc. Japan **51**, 683–691 (1999)

Gamma-Ray Emission from Pulsar Outer Magnetosphere: Spectra of Curvature Radiation

Kouichi HIROTANI
National Astronomical Observatory, Mitaka, Tokyo 181-8588
E-mail (FI): hirotani@hotaka.mtk.nao.ac.jp
and
Shinpei SHIBATA
Department of Physics, Yamagata University, Yamagata, Yamagata 990-8560

(Received 1999 May 7; accepted 1999 August 23)

Abstract

We consider the structure of a stationary outer-gap accelerator around an oblique rotator. Pulsar wind may bring about charge depletion in the magnetosphere near to the light cylinder; the charge depletion, in turn, would cause a large electric field along the magnetic field lines. Positrons or electrons migrating in the gap are accelerated by this field to radiate γ-ray photons by curvature radiation. These γ-ray photons produce yet more radiating particles by colliding with surface blackbody X-ray photons, leading to a pair-production cascade in the gap. The replenished charges partially screen the longitudinal electric field, which is self-consistently solved together with the distribution of $e^{\pm}$'s and γ-ray photons. We find that both the peak energy and the luminosity of γ-rays are a decreasing function of the surface blackbody temperature. Applying the results to PSR B1706 − 44, we can predict that its unobserved X-ray spectrum has a blackbody temperature of about 100 eV.

Key words: Gamma-rays: theory — Magnetic field — Pulsars: general

1. Introduction

The EGRET experiment on the Compton Gamma Ray Observatory has detected pulsed signals from at least six rotation-powered pulsars, which are traditionally known as radio pulsars. γ-rays are particularly important as a direct signature of basic non-thermal processes in pulsar magnetospheres, and potentially should help to discriminate among different models. Interpreting γ-rays should also be less ambiguous compared with non-thermal X-rays.

Attempts to model the production of γ-ray radiation have concentrated on two scenarios: polar-cap models with emission altitudes of $\sim 10^4$ cm to several neutron-star radii over a pulsar polar cap surface (Harding et al. 1978; Daugherty, Harding 1982, 1996; Dermer, Sturner 1994; Sturner et al. 1995; also see Scharlemann et al. 1978 for the slot gap model) and outer-gap models with acceleration occurring in the open field zone located near the light cylinder (Cheng et al. 1986a,b, hereafter CHR; Chiang, Romani 1992, 1994; Romani 1996). Both of these pictures have had some success in reproducing global properties of the observed emission. However, there is an important difference between these two models: A polar-cap accelerator releases very little angular momenta, while an outer-gap one could radiate them efficiently. More specifically, the total angular-momentum loss rate must equal the energy-loss rate divided by the angular velocity of the star, implying an average location of energy loss on the light cylinder (Cohen, Treves 1972; Holloway 1977; Shibata 1995), of which distance from the rotation axis is given by

$$r_{\rm LC} = \frac{c}{\Omega} = 10^{8.5}{\Omega_2}^{-1} \text{ cm}, \tag{1}$$

where Ω_2 denotes the angular frequency of the neutron star Ω in units of 10^2 rad s^{-1}.

On these grounds, the purpose here is to explore a little deeper into the outer-gap models. If the outer magnetosphere is filled with a plasma so that the space-charge density $\rho_{\rm e}$ is equal to the local Goldreich–Julian density [$\equiv \Omega B_z/(2\pi c)$ in non-relativistic limit], then the field-aligned electric field vanishes, where B_z is the component of the magnetic field along the rotational axis. However, the depletion of charge in the Goldreich and Julian model in a region where it could not be resupplied, may cause a vacuum region to develop. Holloway (1973) pointed out the possibility that a region which lacks a plasma is formed around the surface on which the local Goldreich–Julian density $\rho_{\rm GJ}$ changes its sign.

CHR developed a version of an outer-magnetospheric γ-ray emission zone in which acceleration in the Holloway gaps above the null surface brings particles to large

Lorentz factors ($\sim 10^{7.5}$). These primary charges produce high-energy γ-ray photons, some of which collide with soft photons to materialize as secondary pairs. The resulting secondary charges suffer strong synchrotron losses to emit secondary radiation. The secondary photons, in turn, materialize as low-energy tertiary pairs, which were argued to produce the soft tertiary photon bath needed for the original gap closure.

In the outer-magnetosphere picture of Romani and Yadigaroglu (1995), they devoloped a model for the beaming of high-energy γ-ray emission that reproduces the observed properties of individual γ-ray pulsars. Subsequently, Romani (1996) described an emission model for γ-ray pulsars based on curvature radiation-reaction-limited charges in the outer magnetosphere and estimated the efficiency of GeV photon production as a function of such pulsar parameters as pulsar age, magnetic field strength B[G] and magnetic inclination $\alpha_{\rm i}$.

However, few attempts have so far been made to construct a self-consistent electrodynamic structure for outer-gap models. For example, CHR assumed a uniform potential drop so that the acceleration field was $\sim V_{\rm gap}/r_{\rm LC}$, where $V_{\rm gap}$ is the voltage drop in the gap. Subsequently, Romani (1996) assumed its functional form to be $\sim r^{-1}$ and computed γ-ray pulse profiles, spectra, and so on. In polar-cap models, on the other hand, Michel (1991, 1993) investigated the formation of dense charged bunches that can produce coherence at radio frequencies, and analyzed the time development of pair-production discharges assuming a uniform acceleration field.

It was Hirotani and Shibata (1999a, Paper I) who first solved the spatial distribution of $E_{\parallel}$ explicitly together with those of particles ($e^{\pm}$) and γ-ray distribution functions, by solving self-consistently both the Poisson equation for electric potential and the Boltzmann equations of $e^{\pm}$'s and γ-rays (see also Beskin et al. 1992; Hirotani, Okamoto 1998 for the same method applied for a black hole magnetosphere). They considered the outer gap that is immersed in a relatively less luminous background radiation field, in which curvature radiation contributes for γ-ray production. In their subsequent paper (Hirotani, Shibata 1999b, Paper II), they further investigated a gap immersed in a more luminous background radiation field, in which γ-ray photons are produced by inverse Compton scatterings. They revealed that the voltage drop in the gap is not more than 10^{12} V when the X-ray radiation is as less luminous as 10^{36} erg s^{-1} and that the voltage drop is a decreasing function of the X-ray luminosity. In addition, they found a useful expression of the electric field distribution in the gap as a function of the current density; this expression is valid when γ-rays are produced not only by IC scatterings but also by curvature radiation. In their recent paper (Hirotani, Shibata 1999c; hereafter Paper III), they analytically considered a gap-closure condition that a single pair produces one pair in the gap on average and demonstrate that both the peak energy and the luminosity of γ-ray emission are a decreasing function of the surface blackbody temperature.

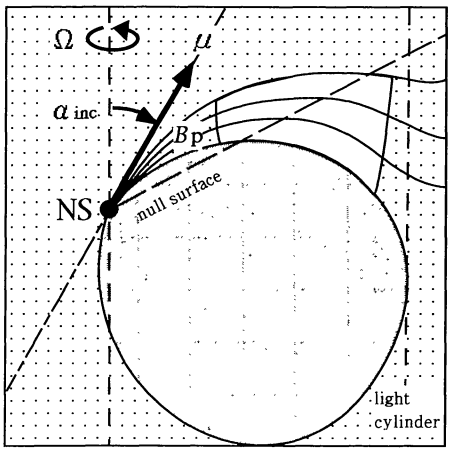

Fig. 1. Side view of a hypothetical outer-magnetospheric gap which is immersed in the surface blackbody X-ray radiation field. γ-ray photons are produced via a curvature radiation process.

In the present paper, we develop the method used in Papers I and III to oblique rotators, taking account of γ-ray spectra explicitly (i.e., discarding the gray approximation). In investigating oblique rotators, without losing any generality, we can choose the sign of $\vec{\Omega}\cdot\vec{\mu}$ to be positive (figure 1), where $\vec{\mu}$ is the magnetic dipole moment. In this case, in the magnetosphere, $\rho_{\rm GJ} < 0$ in the stellar side of the null surface, on which $\rho_{\rm GJ}$ vanishes, and $\rho_{\rm GJ} > 0$ in the equatorial side.

In the next section, we discuss the physical processes of pair production cascade in the outer magnetosphere of a pulsar and present basic equations describing the system. We then solve these equations in section 3 and reveal quantitative characteristics of pair-production cascade. An implication of the results with respect to the unobserved X-ray spectrum of PSR B1706 $-$ 44 is briefly discussed in the final section.

2. Basic Equations and Boundary Conditions

To investigate the gap structure quantitatively, we first reduce the Poisson equation for the electric potential into a one-dimensional form in subsection 2.1. We then give a curvature-limited Lorentz factor in subsection 2.2. This Lorentz factor is essential to quantitatively solve the Boltzmann equations of electrons/positrons in subsection 2.3 and those of γ-ray photons in subsection 2.4. We finally impose suitable boundary conditions in subsection 2.5.

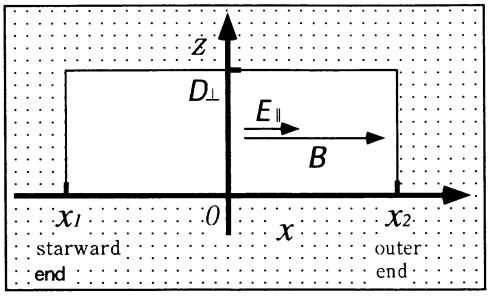

Fig. 2. Rectilinear approximation to the outer gap. The null surface is approximated by the z-axis ($x = 0$). The y-axis, which designates the azimuth, is not depicted to avoid complication.

2.1. *Reduction of the Poisson Equation*

To simplify the geometry, let us introduce a rectilinear approximation for a region around the null surface. Suppose that the magnetic field lines are straight lines parallel to the x-axis (figure 2). Here, x is an outwardly increasing coordinate along a magnetic field line, while y designates the azimuth. We approximate the null surface by the z-axis ($x = 0$). By using this rectilinear coordinates, the Poisson equation for the non-corotating electric potential Φ becomes

$$-\left(\frac{\partial^2}{\partial x^2}+\frac{\partial^2}{\partial y^2}+\frac{\partial^2}{\partial z^2}\right)\Phi(x,y,z) = 4\pi[e(N_+ - N_-) - \rho_{\rm GJ}], \quad (2)$$

where N_+ and N_- are the spatial number densities of e^+'s and e^-'s, respectively; e refers to the magnitude of the charge on the electron. If the trans-field thickness of the gap D_z is sufficiently large compared to the longitudinal thickness of the gap, we can neglect the z-dependence of quantities, that is, $\partial^2/\partial z^2 = 0$. However, D_z, which is determined by quantum electrodynamic processes, can be as large as the longitudinal thickness. To consider these effects, we use an approximation, $\partial^2\Phi/\partial z^2 = -\Phi/{D_z}^2$ (Michel 1974). This approximation stands for the fact that the accelerating region is bounded on $z = 0$ and $z = D_z$ by the side walls on which Φ and hence $E_\parallel$ vanishes.

In the same manner, we Fourier analyze all the quantities in the azimuthal direction and replace $\partial^2/\partial y^2$ with $-m^2$, where m is an integer from the periodic boundary condition. On these grounds, we replace ${\partial_y}^2 + {\partial_z}^2$ with $-{D_\perp}^{-2} \equiv -m^2 - {D_z}^{-2}$ and focus attention on the gap structure in the x direction (i.e., along the magnetic field lines).

The primary effect of field line curvature appears in the x-dependence of $\rho_{\rm GJ}$. Therefore, we adopt the Taylor expansion around the null surface, although we are still in the rectilinear coordinates. Thus, we arrive at the following Poisson equation in the first order approximation:

$$-\frac{d^2\Phi}{dx^2} = -\frac{\Phi}{D_\perp^2} + 4\pi\left[e(N_+ - N_-) - \left(\frac{\partial\rho_{\rm GJ}}{\partial x}\right)_0 x\right], \quad (3)$$

where subscript 0 indicates that the derivative is evaluated at the null surface, $x = 0$.

It is convenient to non-dimensionalize the length scales by a typical Debye scale length $c/\omega_{\rm p}$ (see the discussion in subsection 3.1 in Paper I for details), where

$$\omega_{\rm p} = \sqrt{\frac{4\pi e^2}{m_{\rm e}}\frac{\Omega B}{2\pi c e}} = 1.875\times10^7{\Omega_2}^{1/2}{B_5}^{1/2}\ {\rm rad\ s^{-1}}. \quad (4)$$

First, let us introduce the following dimensionless coordinate variable:

$$\xi \equiv \frac{\omega_{\rm p}}{c}x = 6.25\times10^{-4}{\Omega_2}^{1/2}{B_5}^{1/2}x, \quad (5)$$

where B_5 is the magnetic field at the null surface normalized by 10^5 G; its value is related with the magnetic dipole moment μ and Ω. For the field approximated as a dipole, we obtain

$$B_5 = 0.37\sqrt{1+3\cos^2(\theta_0-\alpha_{\rm i})}\left(\frac{r_0}{r_{\rm LC}}\right)^{-3}\mu_{30}{\Omega_2}^3, \quad (6)$$

where $\mu_{30} \equiv \mu/(10^{30}\ {\rm G\ cm^3})$ and $\alpha_{\rm i}$ refers to the inclination angle of the magnetic moment; (r_0, θ_0) indicates to the polar coordinates of the intersection of the null surface and the last open field line in the poloidal plane. They are defined by

$$\frac{r_0}{r_{\rm LC}} \equiv \frac{4}{4+\tan^2\theta_0}\frac{2\tan^2\alpha_{\rm i}+3+\sqrt{9+8\tan^2\alpha_{\rm i}}}{(4/3)\tan^2\alpha_{\rm i}+3+\sqrt{9+8\tan^2\alpha_{\rm i}}}, \quad (7)$$

$$\tan\theta_0 \equiv \frac{3\tan\alpha_{\rm i}+\sqrt{9\tan^2\alpha_{\rm i}+8}}{2}. \quad (8)$$

To fix the proportionality coefficient, $\xi/x \propto \sqrt{\Omega_2 B_5}$, we evaluate it at the null surface. Its value there depends on the three magnetospheric parameters: Ω, μ, and $\alpha_{\rm i}$. For example, when $\Omega = 10^2$ rad s^{-1} and $\mu = 10^{30}$ G cm^3, we obtain $\xi = 8.31\times10^{-4}x$ if $\alpha_{\rm i} = 0°$, while $\xi = 1.97\times10^{-3}x$ if $\alpha_{\rm i} = 30°$, and $\xi = 4.91\times10^{-4}x$ if $\alpha_{\rm i} = -30°$.

By using ξ, we can simplify the Poisson equation (3) to the form

$$E_\parallel = -\frac{d\varphi}{d\xi} \quad (9)$$

and

$$\frac{dE_\parallel}{d\xi} = -\frac{\varphi}{{\Delta_\perp}^2} + n_+(\xi) - n_-(\xi) - A\xi, \quad (10)$$

where

$$\Delta_\perp \equiv \frac{\omega_{\rm p}}{c}D_\perp; \quad (11)$$

the dimensionless electrostatic potential and electric field are defined by

$$\varphi(\xi) \equiv \frac{e\Phi(x)}{m_e c^2}, \tag{12}$$

$$E_{\parallel} \equiv -\frac{d\varphi}{d\xi} = \frac{e}{m_e c\omega_p}\frac{d\Phi}{dx} \tag{13}$$

$$= 3.12\times10^{-5}\left(\frac{d\Phi/dx}{\mathrm{Vm}^{-1}}\right)\frac{1}{\sqrt{\Omega_2 B_5}}, \tag{14}$$

and the particle densities are normalized in terms of a typical value of the Goldreich–Julian density defined by B (instead of B_z) as follows:

$$n_{\pm}(\xi) \equiv \frac{2\pi ce}{\Omega B}N_{\pm}(x). \tag{15}$$

The dimensionless expansion coefficient of ρ_{GJ}, A, is evaluated at (r_0,θ_0). That is,

$$A \equiv \frac{c}{\omega_p}\frac{2\pi c}{\Omega B}\left(\frac{\partial\rho_{\mathrm{GJ}}}{\partial x}\right)_0$$
$$= 8.00\times10^{-6} f_{\mathrm{A}}(\theta_0,\alpha_i)\frac{r_{\mathrm{LC}}}{r_0}{\Omega_2}^{1/2}{B_5}^{-1/2}, \tag{16}$$

where

$$f_{\mathrm{A}}(\theta_0,\alpha_i) \equiv \sqrt{\frac{4+\tan^2\theta_0}{1+\tan^2\theta_0}}$$
$$\times\left[\frac{3}{2}\sin2\theta_0\cos(\theta_0-\alpha_i)+\cos2\theta_0\sin(\theta_0-\alpha_i)\right]. \tag{17}$$

2.2. *Terminal Lorentz Factor*

The number densities of individual particle species $N_{\pm}$ follow one-dimensional continuity equations with a source term, which is caused by the photon–photon pair production process. The most effective assumption for partile motion in the gap arises from the fact that the velocity immediately saturates in the balance between the radiation reaction force and the electric force. The reaction force is mainly due to curvature radiation if the gap is immersed in a moderate X-ray photon field of which energy density satisfies $U_{\mathrm{x}} < 10^6$ erg cm^{-3} (see subsection 4.2), such as for Vela Pulsar, B1706−44, B1055−52, and Geminga.

In this paper, we consider that the background X-ray field is dominated by surface blackbody radiation with temperature kT. In this case, at a diatance r from the center of the neutron star, U_{x} is related to kT by

$$U_{\mathrm{x}} = 1.5\times10^5\left(\frac{kT}{100\ \mathrm{eV}}\right)^4$$
$$\times{\Omega_2}^2\left(\frac{r}{r_{\mathrm{LC}}}\right)^{-2}\ \mathrm{erg\ cm^{-3}}. \tag{18}$$

Even when the cyclotron resonance scattering contributes, the coefficient on the right-hand side does not increase by an order. Therefore, except for rapid rotators ($\Omega_2 \gg 1$), inverse Compton scatterings can be safely neglected, if the X-ray field is dominated by the surface blackbody radiation, which ensures $U_{\mathrm{x}} < 10^6$ erg cm^{-3}. In Paper I, we parameterized the energy density of X-ray field with U_{x}; instead, we now do it with an observable parameter, kT, in this paper.

Equating the electric force $e|d\Phi/dx|$ and the radiation reaction force with the radius of curvature R_{c}, we obtain the saturated Lorentz factor at each point as follows:

$$\Gamma = \left(\frac{3{R_{\mathrm{c}}}^2}{2e}\left|\frac{d\Phi}{dx}\right| + 10^{24}\right)^{1/4}, \tag{19}$$

where the second term 10^{24} is added for a realistic treatment of the boundaries of the gap. Near the boundaries, where the diminished electric field no longer contributes to the force balance, radiation reaction damps the Lorentz factor. Since the damping length is larger than the width of the boundary regions, Γ is kept over 10^6 in these regions. (Without the 10^{24} term, the vanishing electric field would lead to the vanishment of Γ at the boundaries.)

2.3. *1-D Description of Particle Distribution*

As a first step, we assume a stationary and axisymmetric gap in the present paper. As we shall show in section 3, the gap width along the field lines does not greatly exceed 0.3 r_{LC}, which is much less than the azimuthal length scale πr_{LC}. It seems therefore reasonable to neglect the temporal and azimuthal dependences in the Boltzmann equations for both the particles and the γ-rays.

The mean free path for a γ-ray photon with energy $m_e c^2\epsilon_\gamma$ to collide with the magnetic field with angle q and materialize as a pair is given by (Erber 1966)

$$\lambda_{\mathrm{mag}} \sim \frac{600c}{\omega_{\mathrm{G}}\sin q}\exp\left[\frac{8}{3}\frac{1}{\epsilon_\gamma\sin q}\frac{m_e c^2}{(h/2\pi)\omega_{\mathrm{G}}}\right], \tag{20}$$

where $\omega_{\mathrm{G}} \equiv eB/(m_e c)$. It follows that

$$B \sim \frac{6\times10^{10}}{\sin q}\mathrm{G}\left(\frac{m_e c^2\epsilon_\gamma}{\mathrm{GeV}}\right)^{-1}$$
$$\times\left[\ln\left(\frac{\sin q}{600}\frac{\lambda_{\mathrm{mag}}}{c/\omega_{\mathrm{G}}}\right)\right]^{-1}. \tag{21}$$

Since the logarithm has a value between 20 and 30, we obtain

$$B \geq 2\times10^9 G\left(\frac{m_e c^2\epsilon_\gamma}{\mathrm{GeV}}\right)^{-1}. \tag{22}$$

The equality holds when $\sin q = 1$. Therefore, we can conclude that magnetic pair production becomes important only close to the neutron-star surface. As a result, pairs are produced via γ–γ collisions in the outer-magnetospheric gap.

Bearing this fact in mind, let us now consider the continuity equations of the particles. It should be noted that almost all the particles migrate with the large, saturated Lorentz factor. We therefore assume here that both electrostatic and curvature-radiation-reaction forces cancel out each other to obtain the following continuity equation in the rectilinear coordinates

$$+c\frac{dN_+}{dx} = \int_0^\infty d\epsilon_\gamma \left[\eta_{\rm p+}G_+(x,\epsilon_\gamma)+\eta_{\rm p-}G_-(x,\epsilon_\gamma)\right], \quad (23)$$

$$-c\frac{dN_-}{dx} = \int_0^\infty d\epsilon_\gamma \left[\eta_{\rm p+}G_+(x,\epsilon_\gamma)+\eta_{\rm p-}G_-(x,\epsilon_\gamma)\right], \quad (24)$$

where $N_\pm(x)$ are the spatial number density of $e^\pm$'s, and $G_\pm$ are the distribution function of γ-ray photons having momentum $\pm m_{\rm e}c\epsilon_\gamma$ along the poloidal field line. Since the electric field is assumed to be positive in the gap, e^+'s (or e^-'s) migrate outwards (or inwards). $\eta_{\rm p+}$ (or $\eta_{\rm p-}$) refers to the pair production redistribution function for outward- (or inward-) directed γ-rays. In the framework of the rectilinear approximation, $\eta_{\rm p\pm}$ becomes

$$\eta_{\rm p\pm}(\epsilon_\gamma) \equiv 2.07\times10^4\Omega_2{}^{3/2}B_5{}^{-1/2}\left(\frac{r_{\rm LC}}{r_0}\right)^2 I_\pm(\epsilon_\gamma) \times\left(1-\frac{2c}{\omega_{\rm p}r_{\rm LC}}\frac{r_{\rm LC}}{r_0}\xi\right), \quad (25)$$

where

$$I_\pm(\epsilon_\gamma) = \frac{1}{2}\int_{2/[(1\mp\sin\alpha_{\rm null})\epsilon_\gamma]}^\infty d\epsilon_{\rm x}\frac{\epsilon_{\rm x}^2}{\exp(\epsilon_{\rm x}/\delta)-1} \times\frac{\sigma_{\rm p}(\epsilon_\gamma,\epsilon_{\rm x},\pm\sin\alpha_{\rm null})}{\sigma_{\rm T}}, \quad (26)$$

$$\delta \equiv \frac{kT}{m_{\rm e}c^2} = 1.95\times10^{-4}\left(\frac{kT}{100\,{\rm eV}}\right). \quad (27)$$

Here, $\alpha_{\rm null}$ indicates the angle between the rotational axis and the null surface. For example, $\alpha_{\rm null} = \alpha_{\rm i} = \tan^{-1}\sqrt{2}$ for an aligned rotator. We can derive equation (25) by noting that the colliding angle between an outward- (or inward-) directed γ-rays and a surface X-ray becomes $\pi/2-\alpha_{\rm null}$ (or $\pi/2+\alpha_{\rm null}$) and using a general expression of the redistribution function [equation (21) in Paper II]. The last factor in equation (25) reflects the fact that the X-ray radiation field is diluted by a factor

$$\left(\frac{r}{r_0}\right)^{-2} \approx \left(1+\frac{x}{r_0}\right)^{-2} \approx 1-\frac{2c}{r_0\omega_{\rm p}}\xi. \quad (28)$$

Let us introduce the following dimensionless γ-ray densities in the dimensionless energy interval between β_{i-1} and β_i such that

$$g_\pm{}^i(\xi) \equiv \frac{2\pi ce}{\Omega B}\int_{\beta_{i-1}}^{\beta_i} d\epsilon_\gamma G_\pm(x,\epsilon_\gamma), \quad (29)$$

where $\Omega B/(2\pi ce)$ is a typical value of the Goldreich–Julian number density of particles. In this paper, we set $\beta_0 = 1$, which corresponds to the lowest γ-ray energy, 0.511 MeV. To cover a wide range of γ-ray energies, we divide the γ-ray spectra into 14 energy bins and put $\beta_1 = 3.0$, $\beta_2 = 1.0\times10^1$, $\beta_3 = 3.0\times10^1$, $\beta_4 = 1.0\times10^2$, $\beta_5 = 2.0\times10^2$, $\beta_6 = 3.0\times10^2$, $\beta_7 = 6.0\times10^2$, $\beta_8 = 1.0\times10^3$, $\beta_9 = 2.0\times10^3$, $\beta_{10} = 3.0\times10^3$, $\beta_{11} = 6.0\times10^3$, $\beta_{12} = 1.0\times10^4$, $\beta_{13} = 3.0\times10^4$, $\beta_{14} = 1.0\times10^5$. Provided that the blackbody temperature is roughly 100 eV, only γ-rays having energies

$$m_{\rm e}c^2\epsilon_\gamma > 10^3\left(\frac{kT}{100\,{\rm eV}}\right)^{-1}m_{\rm e}c^2 \approx 0.5\left(\frac{kT}{100\,{\rm eV}}\right)^{-1}{\rm GeV} \quad (30)$$

can contribute for pair production. As shown in subsection 3.3, curvature radiation cannot produce γ-rays that have energies greatly exceed this threshold; therefore, $\beta_{14}m_{\rm e}c^2 = 51.1$ GeV is a safe upper limit.

We can rewrite equations (23) and (24) into the dimensionless forms,

$$\frac{dn_+}{d\xi} = +\sum_{i=1}^{14}[\eta_{\rm p+}^i g_+^i(\xi)+\eta_{\rm p-}^i g_-^i(\xi)] \quad (31)$$

$$\frac{dn_-}{d\xi} = -\sum_{i=1}^{14}[\eta_{\rm p+}^i g_+^i(\xi)+\eta_{\rm p-}^i g_-^i(\xi)], \quad (32)$$

where $\eta_{\rm p\pm}^i$ are evaluated at the central energy in each bin and are defined as

$$\eta_{\rm p\pm}^i \equiv \frac{1}{\omega_{\rm p}}\eta_{\rm p\pm}\left(\frac{\beta_{i-1}+\beta_i}{2}\right); \quad (33)$$

$n_\pm(\xi) \equiv (2\pi ce/\Omega B)N_\pm(x)$ is normalized with the same factor as $g_\pm^i(\xi)$.

A combination of equations (31) and (32) gives the current conservation law,

$$j_0 \equiv n_+(\xi)+n_-(\xi) = \text{constant for } \xi. \quad (34)$$

When $j_0 = 1.0$, the current density equals the typical Goldreich–Julian current density, $\Omega B/(2\pi)$.

2.4. Gamma-Ray Boltzmann Equations

Let us next discuss the Boltzmann equations which the γ-ray distribution functions obey. In the rectilinear approximation, γ-ray photons are considered to be directed only in the $\pm x$-direction due to relativistic beaming. We thus approximate the γ-ray Boltzmann equations into the one-dimensional form

$$\pm c\frac{\partial}{\partial x}G_{\pm}(x,\epsilon_\gamma) = -\eta_{\rm p\pm}G_{\pm}(x,\epsilon_\gamma) + \eta_{\rm c}N_{\pm}(x), \tag{35}$$

where (e.g., Rybicki, Lightman 1979)

$$\eta_{\rm c} \equiv \frac{\sqrt{3}e^2\Gamma}{hR_{\rm c}}\frac{1}{\epsilon_\gamma}F\left(\frac{\epsilon_\gamma}{\epsilon_{\rm c}}\right), \tag{36}$$

$$\epsilon_{\rm c} \equiv \frac{1}{m_{\rm e}c^2}\frac{3}{4\pi}\frac{hc\Gamma^3}{R_{\rm c}}, \tag{37}$$

$$F(s) \equiv s\int_x^\infty K_{\frac{5}{3}}(t)dt, \tag{38}$$

where $R_{\rm c}$ is the curvature radius of the magnetic field lines. The effect of the broad spectrum of curvature γ-rays is represented by the factor $F(\epsilon_\gamma/\epsilon_{\rm c})$ in equation (36).

Integrating (35) in the energy intervals $[\beta_{i-1},\ \beta_i]$, we obtain

$$\pm\frac{d}{d\xi}g^i_{\pm}(\xi) = -\eta_{{\rm p}^i_{\pm}g^i_{\pm}(\xi)+\eta^i_{\rm c}n_{\pm}(\xi)}, \tag{39}$$

where $i = 1, 2, \cdots, m$ and

$$\begin{aligned}\eta^i_{\rm c} &\equiv \frac{\sqrt{3}e^2\Gamma}{\omega_{\rm p}hR_{\rm c}}\int_{\beta_{i-1}/\epsilon_{\rm c}}^{\beta_i/\epsilon_{\rm c}}ds\int_s^\infty K_{\frac{5}{3}}(t)dt \\ &= 2.14\times10^{-8}\Gamma\left(\frac{R_{\rm c}}{0.5r_{\rm LC}}\right)^{-1}\sqrt{\frac{\Omega_2}{B_5}} \\ &\quad\times\int_{\beta_{i-1}/\epsilon_{\rm c}}^{\beta_i/\epsilon_{\rm c}}ds\int_s^\infty K_{\frac{5}{3}}(t)dt.\end{aligned} \tag{40}$$

We may notice here that the ratio

$$\begin{aligned}\frac{\eta^i_{\rm c}}{\eta^i_{\rm p\pm}} &\approx \frac{10^{-8}\Gamma\Omega_2^{1/2}B_5^{-1/2}}{10^4\delta^2\Omega_2^{3/2}B_5^{-1/2}} \\ &\approx 10^3\left(\frac{\Gamma}{10^7}\right)\left(\frac{kT}{100\ {\rm eV}}\right)^{-2}\Omega_2{}^{-1}\end{aligned} \tag{41}$$

is much greater than unity unless Γ is sufficiently less than 10^7. Therefore, the γ-ray production term dominates the γ–γ absorption terms of equation (39).

The migrating $e^\pm$'s and the γ-ray photons in the gap are described by $2m+4$ differential equations (9), (10), (31), (32), and (39). It is worth noting that n^+ and n^- are related through the current conservation relation (34). To solve these equations, we shall impose some boundary conditions in the next subsection.

2.5. Boundary Conditions

Let us first consider the conditions at the *inner* (starward) boundary $\xi = \xi_1$. For one thing, the inner boundary is defined as the place where $E_\parallel$ vanishes. Therefore, we have

$$E_\parallel(\xi_1) = 0. \tag{42}$$

It is noteworthy that condition (42) is consistent with the stability condition at the plasma–vacuum interface if the electrically supported magnetospheric plasma is completely-charge-separated, i.e., if the plasma cloud at $x < x_1$ is composed of electrons alone (Krause-Polstorff, Michel 1985a,b).

Further, we put the value of Φ to be zero at the inner boundary,

$$\varphi(\xi_1) = 0. \tag{43}$$

What is more, we impose for simplicity that no γ-rays capable of pair production enter from the outside of the gap; that is,

$$g^i_+(\xi_1) = 0 \quad (i = 1, 2, \cdots, m). \tag{44}$$

One final point is that we can impose conditions on n_+ and n_-. Assuming the negatively charged cloud at $x < x_1$ is composed of pure electrons, we can expect no influx of positrons, which are migrating $+x$ direction in the gap, at the inner boundary. Therefore, we obtain

$$n_+(\xi_1) = 0, \tag{45}$$

which yields with the help of the charge-conservation law (34),

$$n_-(\xi_1) = j_0. \tag{46}$$

We next consider the conditions at the *outer* boundary. The outer boundary, $\xi = \xi_2$, is defined so that $E_\parallel$ vanishes again. That is,

$$E_\parallel(\xi_2) = 0. \tag{47}$$

In the same manner at $\xi = \xi_1$, we impose both

$$g^i_-(\xi_2) = 0 \quad (i = 1, 2, \cdots, m) \tag{48}$$

and

$$n_-(\xi_2) = 0. \tag{49}$$

We have totally $2m+6$ boundary conditions (42)–(49) for $2m+4$ unknown functions Φ, $E_\parallel$, n_+, n_-, g^1_+, g^2_+, $\cdots$, g^m_+, g^1_-, g^2_-, $\cdots$, g^m_-. Thus two extra boundary conditions must be compensated by making the positions of the boundaries ξ_1 and ξ_2 be free. The two free boundaries appear because $E_\parallel = 0$ is imposed at the *both* boundaries and because j_0 is externally imposed.

In summary, the gap structure is described in terms of the following five dimensionless parameters:

$$j_0 \equiv n_+ + n_-, \tag{50}$$

$$\eta^i_{\rm p\pm} \propto {\Omega_2}^{3/2} {B_5}^{-1/2} I\left(\frac{\beta_i + \beta_{i-1}}{2}\right), \tag{51}$$

$$\eta^i_{\rm c} \propto \frac{R_{\rm c}}{c/\omega_{\rm p}}, \tag{52}$$

$$\Delta_\perp \equiv D_\perp/(c/\omega_{\rm p}) \propto D_\perp(\Omega B)^{-1/2}, \tag{53}$$

$$\alpha_{\rm i}. \tag{54}$$

The surface temperature, kT, appears through the integral I in equation (51) or (26), whereas the inclination angle $\alpha_{\rm i}$ apprears through the expansion coefficient A in equation (16) and through the functions $r_0/r_{\rm LC}$ and θ_0. It is important that j_0 is a free parameter in this paper, because it can be determined only from a global condition of the current circuit (e.g., Shibata 1997).

3. Results

3.1. Electric Field Structure

As a beginning, we examine how $E_\parallel(\xi)$ depends on the 'first' parameter j_0 [equation (50)]. In figure 3, we show some examples of $E_\parallel(\xi)$; the dotted, dashed, and solid lines correspond to $j_0 = 0.218$, $j_0 = 0.20$, and $j_0 = 0.10$, respectively. The other parameters are fixed as $\Omega_2 = 1.0$, $\mu_{30} = 1.0$, $kT = 75$ eV, $D_8 \equiv D_\perp/10^8$ cm $= 1.0$, $R_{\rm C} = 0.5\ r_{\rm LC}$, and $\alpha_{\rm i} = 0$, so that the remaining four parameters (51)–(54) are not changed at all.

For very small j_0, the $n_+ - n_-$ term in equation (10) does not contribute. Moreover, unless the gap width, $H \equiv \xi_2 - \xi_1$, exceeds $\Delta_\perp = 6.25 \times 10^4 D_8 \sqrt{\Omega_2 B_5}$, the first term $-\varphi/{\Delta_\perp}^2$, which describes the 2-dimensional effect in the Maxwell equation, is not important either. As a result, equation (10) gives approximately a quadratic solution,

$$E_\parallel(\xi) = E_\parallel(0) - (A/2)\xi^2. \tag{55}$$

In figure 3, the solid line (small j_0 case) approximately represents such a quadratic solution. Since the trans-field thickness ($= 10^8$ cm) is comparable with the longitudinal gap width, the two-dimensional effect represented by $-\varphi/{\Delta_\perp}^2$ term in equation (10) contributes to shift the gap outwards.

However, as j_0 increases, $E_\parallel(\xi)$ deviates from the quadratic form to have a 'brim' at the inner boundary. And at last, at a certain value, $j_0 = j_{\rm cr}$, the derivative of $E_\parallel$ vanishes at the inner boundary. In the case of $\Omega_2 = 1.0$, $\mu_{30} = 1.0$, $kT = 75$ eV, $D_8 = 1.0$, and $\alpha_{\rm i} = 0$, $j_{\rm cr}$ equals 0.218, for which the solution is represented by the dotted line in figure 3. Above the critical current density, $j_{\rm cr}$, there are no solutions satisfying the boundary conditions presented in subsection 2.5.

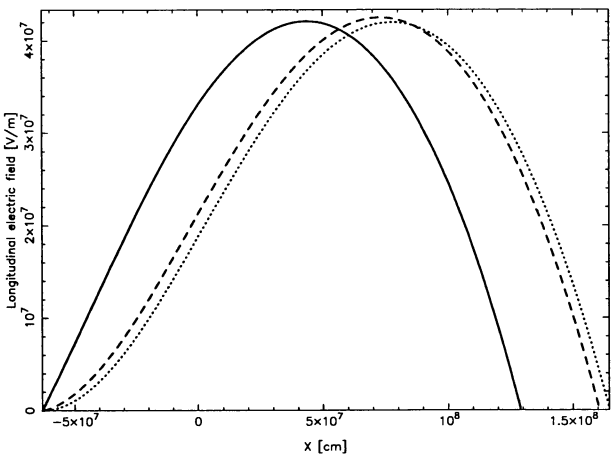

Fig. 3. Examples of longitudinal electric field $E_\parallel(x)$. The dotted, dashed, and solid lines represent the solution corresponding to $j_0 = 0.218$, $j_0 = 0.20$, and $j_0 = 0.10$, respectively. The other parameters are fixed as $\Omega_2 = 1.0$, $\mu_{30} = 1.0$, $D_8 = 1.0$, and $kT = 75$ eV throughout the gap.

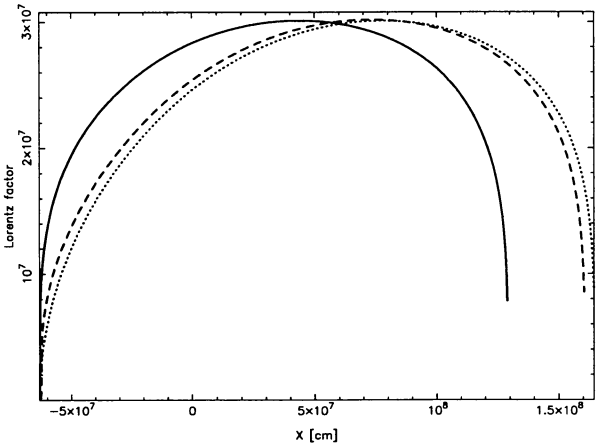

Fig. 4. Examples of the Lorentz factor $\Gamma(\xi)$. The solid, dashed, and dotted lines correspond to the same parameters chosen in figure 3.

It will also be useful to describe the Lorentz factor $\Gamma(\xi)$. The results are presented in figure 4; the parameters are the same as we have chosen in figure 3. As figure 4 indicates, the typical values of Γ become $\sim 10^{7.2}$ in the most part of the gap, except the case when j_0 is very much close to $j_{\rm cr}$. It is noteworthy that $e^\pm$'s with $\Gamma \sim 10^{7.2}$ produce γ-ray photons of energy $\epsilon_\gamma \approx 3hc\Gamma^3/(2\pi r_{\rm LC}) \sim$ GeV, which are most effectively collide with soft X-ray photons ($m_{\rm e}c^2\epsilon_{\rm x} < 1$ keV) to produce pairs.

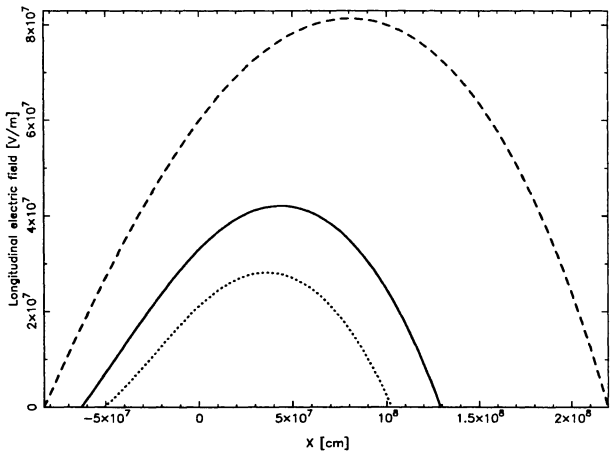

Fig. 5. Examples of the longitudinal electric field, $E_{\parallel}(x)$. The dotted, solid, and dashed lines represent the solution corresponding to kT = 100, 75, and 50 eV, respectively. The other parameters are fixed as $\Omega = 60$ rad s^{-1}, $\mu_{30} = 1.0$, $D_8 = 1.0$, and $j_0 = 0.1$.

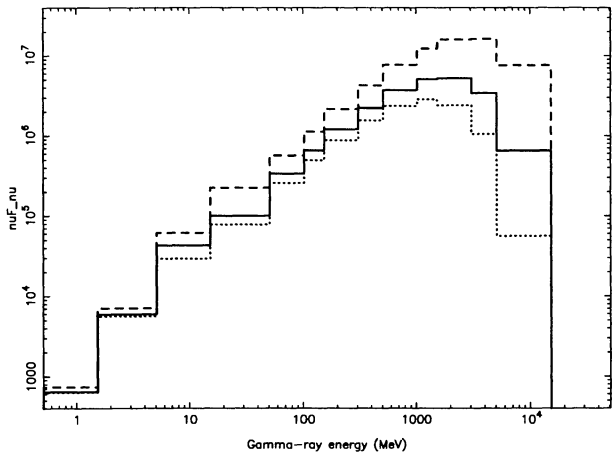

Fig. 6. Curvature γ-ray spectra as a function of surface blackbody temperature, kT. The dashed, solid, and dotted lines correspond to kT = 50, 75, and 100 eV, respectively.

3.2. *Electric Field vs. Surface Temperature*

We next investigate how the strength of $E_{\parallel}(\xi)$ depends on kT. In figure 5, we compare the results of three cases: The thick line corresponds to kT = 75 eV, while the dashed and dotted ones to 50 and 100 eV, respectively. The other paramters are fixed as $j_0 = 0.1$, $\Omega = 60$ rad s^{-1}, $\mu = 10^{30}$ G cm^{-3}, and $\alpha_{\rm i} = 30°$. It follows from this figure that the maximum value of $E_{\parallel}$ reaches $10^{8.0}$ V m^{-1} for kT = 50 eV but does only $10^{7.4}$ V m^{-1} for 100 eV. That is, $E_{\parallel}$ is a decreasing function of kT. The reason is as follows: If kT increases, the target photons for pair production increases. This in turn reduces the pair-production mean-free path, and hence the gap width. Since $E_{\parallel}$ is roughly proportional to the square of the gap width [equation (55)], the increase in kT results in a decrease in $E_{\parallel}$.

Integrating $E_{\parallel}$ from ξ_1 to ξ_2, we can further discuss the voltage drop in the gap. For $kT \sim 50$ eV, the voltage drop becomes roughly $10^{14.2}$ Volts, which attains about 15% of the neutron star surface EMF, $10^{15}[\Omega(60 \text{ rad s}^{-1})^{-1}]^2\mu_{30}$ Volts.

3.3. *Gamma-Ray Spectrum*

Let us finally examine the spectrum of curvature-radiated γ-rays. We present the γ-ray spectra as a function of the surface blackbody temperature kT in figure 6. The dashed, solid, and dotted lines correspond to kT = 50, 75, and 100 eV, respectively. The other parameters are fixed as $j_0 = 0.1$, $\Omega = 60$ rad s^{-1}, $\mu_{30} = 10^{30}$ G cm^3, $D_\perp = 10^8$ cm, $R_{\rm C} = 0.5\, r_{\rm LC}$, and $\alpha_{\rm i} = 0°$. It is plain from figure 6 that the γ-ray spectra peak around GeV and that both the peak energy and luminosity increase with decreasing kT. The reason for this behavior is that a decrease in kT results in a decrease in the X-ray energy density, which reduces the drag force due to curvature radiation, thereby increasing the terminal Lorentz factor and hence γ-ray energies. For more details, see the explanation in section 3 of Paper III. The peak energy is consistent with observations. The luminosity would be also consistent with observations if we computed it in the same manner as in section 3 of Paper III.

Let us next demonstrate how the γ-ray spectrum depends on the inclination angle $\alpha_{\rm i}$. In figure 7, we present the γ-ray flux as a function of j_0 and $\alpha_{\rm i}$. The solid, dashed, and dotted lines correspond to $\alpha_{\rm i} = 0°$, $-30°$, and $30°$, respectively. We set $j_0 = 0.1$. It follows that the γ-ray flux does not significantly depends on $\alpha_{\rm i}$. The reason is as follows: If $\alpha_{\rm i}$ increases for instance, the gap moves inwards. This results in the increase of target photons, which reduces the pair production mean-free path $\lambda_{\rm p}$. It should be noted that the increase of $\alpha_{\rm i}$ has a counter effect, resulting in a decrease of the collision angles between the outward-directed γ-rays and the soft photons, which enlarges $\lambda_{\rm p}$. These two effects cancel each other, and the gap structure is relatively unaffected by the variation in $\alpha_{\rm i}$.

4. Discussion

In summary, we have developed a one-dimensional model for an outer-gap accelerator immersed in a surface X-ray radiation field of middle-aged pulsars, of which the energy density becomes not less than 10^6 erg cm^{-3} for

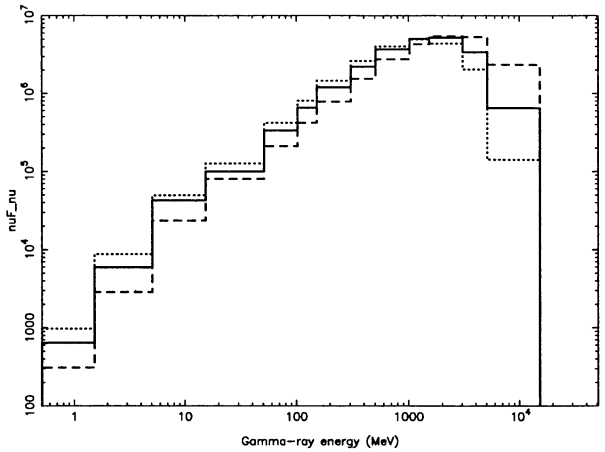

Fig. 7. Curvature γ-ray spectra as a function of the inclination angle, α_i. The solid, dashed, and dotted lines correspond to $\alpha_i = 0°$, $-30°$, and $30°$, respectively. Current density is fixed as $j_0 = 0.1$.

$kT < 100$ eV. The equilibrium Lorentz factor becomes somewhat larger than 10^7. For such a large Lorentz factor, the curvature radiation becomes the dominant process in γ-ray production. As the X-ray radiation field becomes less luminous, the pair-production mean-free path, and hence H, increases. The voltage drop can attain 30% of the surface EMF if kT is as small as 50 eV. We find that both the peak energy and the luminosity of γ-rays are a decreasing function of the surface blackbody temperature and that they do not depend on the inclination very much.

Let us show the validity of assumptions that have been made in this paper. We must check that the acceleration length l_{acc} is sufficiently less than the gap width, so that most of the particles attain the terminal Lorentz factor [equation (19)]. Evaluating $l_{acc} = \Gamma m_e c^2/eE_\parallel$, we find that the ratio l_{acc}/H is an increasing function of kT and is less than unity for $kT < 100$ eV. Again, the ratios of l_{acc} and the gap width are consistent with the semi-analytic estimate in Paper III.

Let us finally discuss the implication for X-ray spectrum of PSR B1706 $-$ 44. The theory of curvature radiation tells that the peak energy is about $E_c \propto \Gamma^3/R_c \propto E_\parallel^{3/4} R_c^{1/2}$. As we have seen, $E_\parallel$ is a decreasing function of kT, because the number density of target soft photons increases with increasing kT. Figures 6 and 7 show that the curvature spectrum peaks at several GeV, which is consistent with the observations of Vela Pulsar, B1706 $-$ 44, and Geminga. (The spectrum of B1055 $-$ 52 above GeV is unknown.) Since the γ-ray spectrum of B1706 $-$ 44 peaks at 1.3 GeV, our analysis leads to the conclusion that the surface temperature of B1706 $-$ 44, of which X-ray spectrum has not been reported, is about 100 eV.

The authors thank the Astronomical Data Analysis Center of National Astronomical Observatory for the use of workstations. This work was supported in part by Grant-in-Aid for Scientific Research from the Ministry of Education, Science, Sports and Culture (09680468, 08454047, and 10117203).

References

Beskin V.S., Istomin Ya.N., Par'ev V.I. 1992, Sov. Astron. 36, 642
Cheng K.S., Ho C., Ruderman M. 1986a, ApJ 300, 500 (CHR86a)
Cheng K.S., Ho C., Ruderman M. 1986b, ApJ 300, 522 (CHR86b)
Chiang J., Romani R.W. 1992, ApJ 400, 629
Chiang J., Romani R.W. 1994, ApJ 436, 754
Cohen R.H., Treves A. 1972, A&A 20, 305
Daugherty J., Harding A.K. 1982, ApJ 252, 337
Daugherty J., Harding A.K. 1996, ApJ 458, 278
Dermer C.D., Sturner S.I. 1994, ApJ 420, L75
Erber T. 1966, Rev. Mod. Phys. 38, 626
Harding A.K., Tademaru E., Esposito L.S. 1978, ApJ 225, 226
Hirotani K., Okamoto I. 1998, ApJ 497, 563
Hirotani K., Shibata S. 1999a, MNRAS 308, 54 (Paper I)
Hirotani K., Shibata S. 1999b, MNRAS 308, 67 (Paper II)
Hirotani K., Shibata S. 1999c, MNRAS submitted (Paper III)
Holloway N.J. 1973, Nature 246, 6
Holloway N.J. 1977, MNRAS 18, 19
Krause-Polstorff J., Michel F.C. 1985a, MNRAS 213, 43
Krause-Polstorff J., Michel F.C. 1985b, A&A 144, 72
Michel F.C. 1974, ApJ 192, 713
Michel F.C. 1991, ApJ 383, 808
Michel F.C. 1993, in Proc. Los Alamos Workshop, ed K.A. Van Riper, R. Epstein, C. Ho (Cambridge University Press) p202
Romani R.W. 1996, ApJ 470, 469
Romani R.W., Yadigaroglu I. 1995, ApJ 438, 314
Rybicki G.B., Lightman A.P. 1979, Radiative processes in astrophysics (John Wiley & Sons, New York)
Scharlemann E.T., Arons J., Fawley W.M. 1978, ApJ 222, 297
Shibata S. 1995, MNRAS 276, 537
Shibata S. 1997, MNRAS 287, 262
Sturner S.J., Dermer C.D., Michel F.C. 1995, ApJ 445, 736